

# Analysis of clinical, dosimetric and radiomic features for predicting local failure after stereotactic radiotherapy of brain metastases in malignant melanoma

**Authors:** Hartong Nanna E.<sup>1,7</sup> MD, Sachpazidis Ilias<sup>2,7</sup> PhD, Blanck Oliver<sup>3</sup> PhD, Etzel Lucas<sup>4</sup> MD, Peeken Jan C.<sup>4</sup> MD, Combs Stephanie E.<sup>4</sup> MD, Urbach Horst<sup>5</sup> MD, Zaitsev Maxim<sup>6,7</sup> PhD, Baltas Dimos<sup>2,7</sup> PhD, Popp Ilinca<sup>1,7</sup> MD, Grosu Anca-Ligia<sup>1,7</sup> MD, Fechter Tobias<sup>2,7</sup> PhD

<sup>1</sup> Department of Radiation Oncology, Medical Center University of Freiburg, Faculty of Medicine. University of Freiburg, Germany

<sup>2</sup> Division of Medical Physics, Department of Radiation Oncology, Medical Center University of Freiburg, Faculty of Medicine, University of Freiburg, Germany

<sup>3</sup> Department of Radiation Oncology, University Medical Center Schleswig-Holstein, Kiel, Germany

<sup>4</sup> Department of Radiation Oncology, Klinikum Rechts der Isar, Technical University of Munich (TUM), Munich, Germany

<sup>5</sup> Department of Neuroradiology, Medical Center University of Freiburg, Faculty of Medicine. University of Freiburg, Germany

<sup>6</sup> Division of Medical Physics, Department of Diagnostic and Interventional Radiology, Medical Center University of Freiburg, Faculty of Medicine. University of Freiburg, Germany

<sup>7</sup> German Cancer Consortium (DKTK). Partner Site Freiburg, Germany

## Abstract:

**Background:** The aim of this study was to investigate the role of clinical, dosimetric and pretherapeutic magnetic resonance imaging (MRI) features for lesion-specific outcome prediction of stereotactic radiotherapy (SRT) in patients with brain metastases from malignant melanoma (MBM).

**Methods:** In this multicenter, retrospective analysis, we reviewed 517 MBM from 130 patients treated with SRT (single fraction or hypofractionated). For each gross tumor volume (GTV) 1576 radiomic features (RF) were calculated (788 each for the GTV and for a 3 mm margin around the GTV). Clinical parameters, radiation dose and RF from pretherapeutic contrast-enhanced T1-weighted MRI from different institutions were evaluated with a feature processing and elimination pipeline in a nested cross-validation scheme.

**Results:** Seventy-two (72) of 517 lesions (13.9%) showed a local failure (LF) after SRT. The processing pipeline showed clinical, dosimetric and radiomic features providing information for LF prediction. The most prominent ones were the correlation of the gray level co-occurrence matrix of the margin (hazard ratio (HR): 0.37, confidence interval (CI): 0.23-0.58) and systemic therapy before SRT (HR: 0.55, CI: 0.42-0.70). The majority of RF associated with LF was calculated in the margin around the GTV.

**Conclusions:** Pretherapeutic MRI based RF connected with lesion-specific outcome after SRT could be identified, despite multicentric data and minor differences in imaging protocols. Image data analysis of the surrounding metastatic environment may provide therapy-relevant information with the potential to further individualize radiotherapy strategies.

**Keywords:** malignant melanoma, brain metastasis, stereotactic radiotherapy, radiomics, machine learning

## 1.0 INTRODUCTION

Malignant melanoma is one of the most common causes of brain metastases. Nearly 50% of patients with stage IV disease develop brain metastases (1). In recent years, earlier detection through improved imaging techniques, more effective local treatment options and novel systemic agents have significantly improved the historically poor prognosis of melanoma brain metastases (MBM) (2) and increased the number of patients with long-term disease control (3).

Despite this positive trend, MBM remains a common cause of intracranial failure and neurological death, even in the context of controlled or absent extracranial disease (4). Brain metastases from melanoma are more likely to cause neurological death than those from lung, breast and gastrointestinal cancers (5). This highlights the critical importance of the local therapy for MBM (6,7).

Radiation therapy is a key component in the local treatment of MBM. MBM can be effectively treated with local, stereotactic radiotherapy (SRT – radiosurgery, SRS or stereotactic fractionated radiotherapy, SFRT) with one-year control rates of 60-80% (8,9). In particular, patients with a solitary and oligometastatic disease amenable to SRS are associated with improved survival (10). Even with 10 or more MBM, SRS (without WBRT) can lead to a high level of intracranial tumor control (11). If whole brain radiation therapy (WBRT) is necessary, the hippocampal sparing treatment can significantly avoid the cognitive deficits after WBRT (12).

Patient-specific prognostic factors have been repeatedly investigated (13). For example, Bian et al. identified a greater lesion number, higher intracranial tumor volume, and older age as negative prognostic factors for survival after SRT for MBM (14). Stera et al. showed that both the application of immunotherapy and systemic therapy before or concomitant to SRS were associated with improved overall survival (15). However, these factors cannot predict the local treatment response.

It is conceivable that lesions that develop local failure (LF) show specific characteristics on medical imaging. Both visible and invisible features can be statistically evaluated using radiomic features (RF) analysis. RF analysis is an emerging area of translational research that involves the extraction of a large number of quantitative features from clinical imaging (16). Bhatia and colleagues identified magnetic resonance imaging (MRI) features associated with survival in MBM treated with immune checkpoint inhibitors and suggested that RF are potential biomarkers to predict intratumoral heterogeneity and risk of intracranial progression (17).

*A priori* knowledge of lesion-specific outcome may contribute to a more individualized treatment, including risk-adapted target volume delineation or dose (de-)escalation techniques. The aim of our study was to investigate the predictive power of clinical, dosimetric and MRI features in estimating the lesion-specific outcome of MBM following SRT using machine learning. Developed code, radiomic features and models are publicly available: <https://github.com/ToFec/RadiomicsMM>.

## 2.0 MATERIALS & METHODS

The primary outcome is LF, defined per lesion as in-field progression according to the Response Assessment in Neuro-Oncology brain metastases (RANO-BM) criteria (18). LF was assessed by MRI 6-8 weeks and then every 3 months after treatment with a minimum follow-up of 12 weeks. Multivariate Cox proportional hazard models (CPHMs) (19) were fitted with clinical, dosimetric and image features to model the lesion-specific risk of LF. The study was approved by the local ethics committee of the Medical Faculty of the University of Freiburg (registered under the sign 20-1031\_3).

### 2.1 Clinical and dosimetric characteristics

In this multicenter, retrospective analysis, we included neuroimaging, clinical and dosimetric data on 517 metastases from 130 patients who received 179 series of SRT for MBM. Radiotherapy specifications are summarized in Table 1. The majority of patients received SRT as SRS or in combination with WBRT. In this case, the metastatic lesions were treated with 51 Gy/12 fractions with hippocampus avoidance, according to the protocol of the HIPPORAD trial (20). Treatment was delivered in three primary care centers. Criteria to include the patients into the analysis were as follows: (a) local radiotherapy for brain metastases from pathologically confirmed malignant melanoma between 2012 and 2021; (b) age 18 years or older; (c) pretherapeutic contrast-enhanced MRI; (d) minimum biologically equivalent dose (BED) of 41 Gy ( $\alpha/\beta=10$  Gy). Lesions with prior neurosurgical or radiation treatment were excluded from the analysis. Clinical parameters are summarized in Table 2. The following initial clinical and dose features were evaluated: age, gender, Karnofsky performance scale, systemic therapy before (>14 days), during (within 14 days) and after (>14 days) radiotherapy, molecular targets, melanoma-specific grade prognostic assessment score (molGPA) at time of MBM diagnosis (13), number of brain metastases and type of radiotherapy (SRT as SRS or in combination with WBRT), minimum dose, maximum dose ( $D_{max}$ ), mean dose, D50 Gy, D98 Gy, D2 Gy.

### 2.2 Image-based features

Radiomic features of the images were analyzed to determine which information in MR images is predictive of LF. In this subsection, image acquisition is described first, followed by preprocessing, contouring and RF calculation.

MRI was performed at the three institutions using different MR scanners and acquisition parameters (supplementary material I). To account for different imaging protocols and to standardize the feature extraction all MR images were subjected to the following pre-processing steps: First, bias field correction (21) was performed using ANTs software v2.3.5 (22). All datasets were then resampled to a voxel length of 1 mm in each dimension and the voxel intensities were adjusted within an automatically generated brain mask (FSL brain extraction tool v6.0 (23)) using Z-score normalization.

The initial set of contours encompassed the original gross tumor volume (GTV) and was manually delineated by different radiation oncologists on the 3D-GdT1w-MRI obtained for radiotherapy planning in each patient. An expert radiation oncologist reviewed all contours prior to analysis. As many RF are prone to inter-observer variability but getting additional manual contours is very time-consuming, three artificial contour datasets in addition to the manual GTV contours (ExpCont) were created (Figure 1). One artificial contour dataset (UnetCont) was calculated by facilitating an in-house trained nnUnet (24). The other two artificial contour

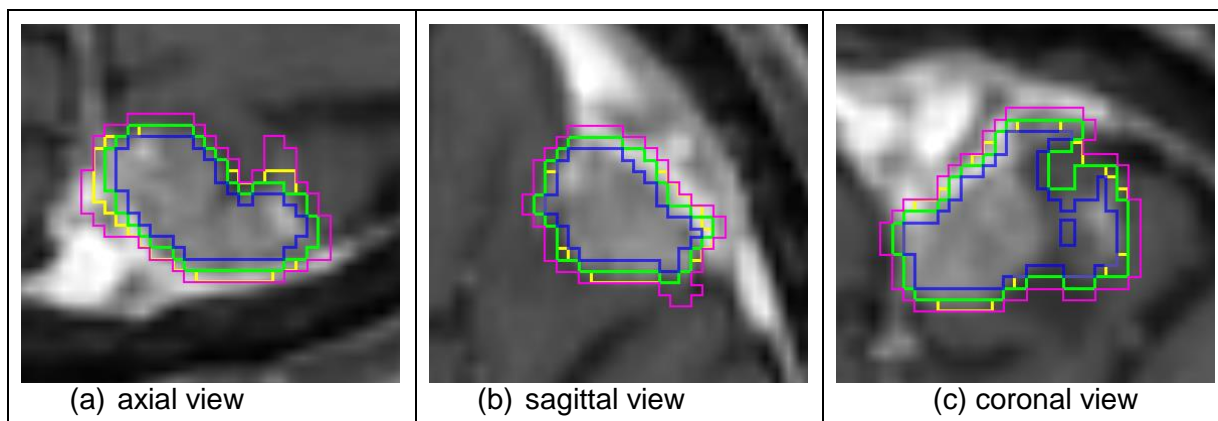


Figure 1: Axial (a), sagittal (b) and coronal (c) views of the contours used to simulate inter-observer variability. The expert contour is shown in green, the nnUnet contour is shown in yellow and the expert contour with erosion or dilation is shown in blue and pink, respectively.

datasets (MorphCont1, MorphCont2) were created by randomly applying either a morphological erosion, morphological dilation or identity function to the contours in ExpCont. More details are given in the supplementary material II.

RF were calculated for the segmented tumor and an isotropic margin of 3 mm around the tumor to include microscopic infiltrations (25) using Pyradiomics v3.0.1 (26). A total of 1576 RF were calculated for each contour, 788 each for tumor and margin.

Table 1 – Radiotherapy specifications per lesion. <i>Abbreviations:</i> BED = biologically effective dose, SRT = stereotactic radiotherapy, SRS = stereotactic radiosurgery, SFRT = stereotactic fractionated radiotherapy				
	Total number of lesions (n=517)	Center I (n=247)	Center II (n=226)	Center III (n=44)
Stereotactic radiosurgery (SRS)	349	93	218	38
SFRT 12-14 fractions	147	147	0	0
SFRT 2-4 fractions	21	7	8	6
SRS dose (median, range)	20 (16-20) Gy	20 (18-20) Gy	18 (16-20) Gy	20 (18-20) Gy
SFRT dose (median, range)	51 (24-51) Gy à 4.25 (3-8) Gy	51 (35-51) Gy à 4.25 (3-5) Gy	24 Gy à 8 Gy	35 Gy à 5 Gy
BED $\alpha/\beta=2$ Gy (median, range)	180 (97.5-220) Gy	159.4 (97.5-220) Gy	180 (120-220) Gy	220 (122.5-220) Gy
BED $\alpha/\beta=10$ Gy (median, range)	60 (41.6-72.7) Gy	72.7 (50.4-72.7) Gy	50.4 (41.6-60) Gy	60 (50.4-60) Gy
Number of fractions (median, range)	1 (1-14)	12 (1-14)	1 (1-3)	1 (1-7)

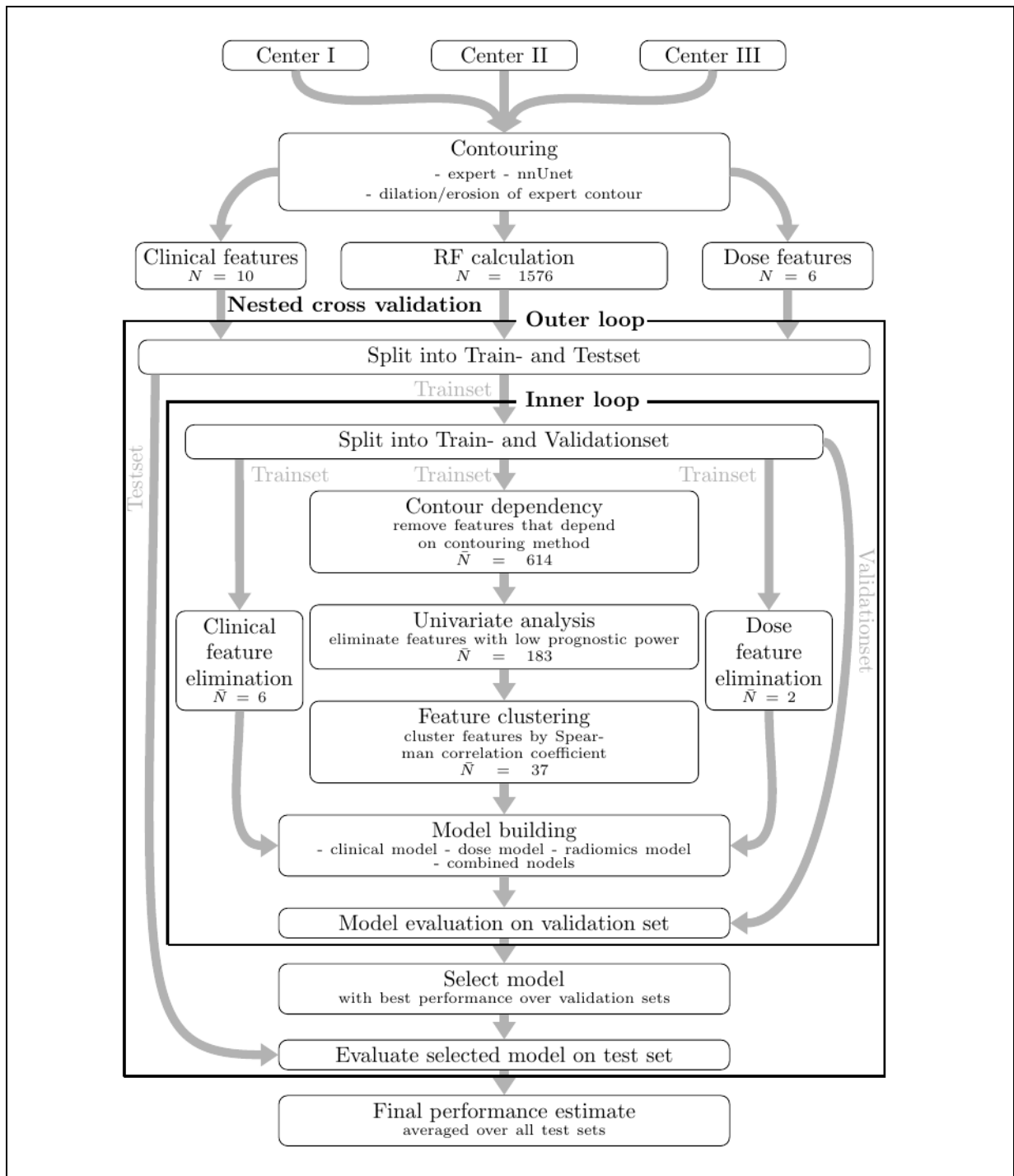


Figure 2: In a first step the data sets were merged, and four contour sets were created for each lesion. Radiomic, dose and clinical features were then calculated or collected. Feature elimination and model building was done in a 30x30 nested cross validation scheme. In the inner loop redundant and contour dependent features were removed and Cox proportional hazards models were fitted and ranked on train and validation sets, respectively. The best model of each inner loop iteration was then evaluated on the test set of the respective outer loop. The final performance estimate was the concordance index averaged over all 30 outer loop iterations.

### 2.3 Feature elimination and model-building

As the number of available features surpasses by far the number of lesions, several measures were taken to mitigate the risk of overfitting. The entire processing pipeline is shown in Figure 2.

For feature elimination, model building and model evaluation a 30x30 nested cross-validation scheme (27) was employed: In an outer loop the entire dataset is divided 30 times into a training set and a test set (80:20). Each training set of the outer loop is further split 30 times into training set and validation set (80:20) in an inner loop. The inner loop's training sets are used for feature elimination and modelling, the validation sets of the inner loop are used for model ranking. The best model is then evaluated on the test set of the outer loop. The final performance estimate of the processing pipeline is the average performance over all 30 test sets of the outer loop. This methodology enables an independent evaluation of selected models. The datasets were disjoint at the patient level, ensuring that a single patient's lesions were not present in both sets.

Table 2 - Demographics per series. <i>Abbreviations:</i> BM = brain metastases; GPA = grade prognostic assessment score; KPS = Karnofsky performance scale; NA: not available; RT = radiotherapy. *= Systemic therapy was defined as chemotherapy, immunotherapy or targeted therapy before (>14 days before), during (within 14 days before or after RT) and after (>14 days after) radiotherapy				
Institution	Total (n=179)	Center I (n=83)	Center II (n=77)	Center III (n=19)
Number of lesions	517	247	226	44
Sex (female/male)	63/116	28/55	27/50	8/11
Age at start of RT (mean ± SD)	61.94 ±14.2 Y	59.93 ±14.58 Y	63.85 ±13.58 Y	62.94 ±14.71 Y
KPS				
90-100%	134	66	61	7
70-80%	38	16	13	9
60%	7	1	3	3
Number of BM (series)				
1	55	22	26	7
2-3	54	20	26	8
4 or more	70	41	25	4
Melanoma molGPA				
0-1	26	19	7	NA
1.5-2	74	43	31	NA
2.5-3	41	17	24	NA
3.5-4	19	4	15	NA

Molecular target				
BRAF-mutation	87	47	31	9
NRAS	23	14	8	1
no driver mutation	69	22	38	9
Systemic therapy*				
before RT (yes/no/NA)	116/44/21	44/40/0	64/4/10	8/0/11
during RT (yes/no/NA )	113/47/21	42/41/1	63/6/13	12/0/7
after RT (yes/no/NA)	136/27/18	53/27/4	65/0/13	18/0/1
Immunotherapy				
before RT (yes/no/NA)	81/91/9	23/61/0	50/19/9	8/11/0
during RT (yes/no/NA)	86/84/11	26/58/0	48/19/11	12/7/0
after RT (yes/no/NA)	112/57/12	40/44/0	55/11/12	17/2/0

Note that the result of the nested CV is a performance estimation of the processing pipeline and not a of a single model (27). To determine one final model, the inner loop model selection was applied to the whole dataset, followed by training the selected model on the entire dataset.

Before each modelling step, features with high variability, redundancy or a low correlation with LF on the inner loop's training set were eliminated. In the main manuscript only a brief overview is given, more details can be found in the supplementary material III. RF were reduced by the following steps: 1) eliminate all features that show a contour dependency 2) remove features with a univariate analysis 3) cluster correlated features. Clinical and dosimetric features were eliminated using only the univariate analysis.

The algorithm for building a multivariate CPHM was as follows: First univariate models were fitted on the training set with the features remaining after feature elimination. The model with the highest concordance index (c-index) on the validation set was then selected, and the algorithm assessed whether the c-index could be increased by an additional feature. Features were added until the maximum number of model features (four) was reached or no further improvement in c-index was possible.

Four different model types were fitted to estimate the risk of LF using the processing pipeline: three using only clinical, dosimetric or radiomic features, respectively, and one using a combination of these.

## 2.4 Statistical details

Statistical analysis was performed using R v4.1.2. Distributions were compared using the Wilcoxon signed-rank test. In all experiments, the confidence alpha was 5%. In the experiments analyzing the contour dependence of the RF, the confidence alpha was set to 10% to further reduce the number of remaining features.

## 3.0 RESULTS

### 3.1 Clinical and dosimetric characteristics

The median age of patients was 61 years (range 23-88) and the median number of BMs at the start of SRT was 3 (range 1-30). LF after SRT occurred in 72 out of 517 lesions (13.9%) at a mean of 6.6 months. Out of 179 series, LF occurred in 40 series (22.3%). 33 out of 130 patients had at least one lesion with LF (25.4%). The local tumor control rate was 88.6% at 12 months. Median survival time was 16.3 months with a median LF-free survival of 13.4 months.

### 3.2 Model-building and analysis

We compared the performance of the processing pipeline with four different model types: three based solely on clinical, dosimetric or radiomic features, and one used a combination of all features.

When processing only clinical features with the pipeline, information about systemic treatment before (SysBefore) and during (SysDuring) RT seemed the most relevant for predicting local failure. SysBefore and SysDuring were part of the selected models in 18 and 13 out of 30 outer loop iterations, respectively. The mean hazard ratio (HR) with standard deviation was 0.41 +/- 0.06 for SysBefore and 0.39 +/- 0.04 for SysDuring. Beside the systemic therapy, gender and age need to be noted, being present in 47% and 40% of the models, with HRs of 0.40 +/- 0.07 for gender and 0.76 +/- 0.06 for age. The overall performance of the processing pipeline using only clinical features showed a mean c-index of 0.58 +/- 0.13. The final model which was trained on the whole dataset consisted of the following features: SysBefore (HR: 0.53, 95% confidence interval (CI): 0.31-0.89, p: 0.02), SysDuring (HR: 0.51, CI: 0.30-0.87, p: 0.01), gender (HR: 0.39, CI: 0.25-0.63, p: 1e-4).

Processing only dosimetric features yielded an overall mean c-index of 0.55 +/- 0.13. A feature representing the maximum dose a lesion received (either in form of  $D_{max}$  or  $D_{2\%}$ , BED  $\alpha/\beta=10$  Gy) was present in all but 6 selected models with a HR of 0.60 +/- 0.23. The final model contained only  $D_{max}$  (HR: 0.68, CI: 0.52-0.88, p: 4e-3).

Feeding the pipeline with just radiomic features showed a mean c-index of 0.62 +/- 0.10. By far the most prominent feature, present in 21 out of 30 selected models was Margin\_wavelet.LLH\_glcm\_Correlation with a mean HR of 0.52 +/- 0.05. The second most feature was present in only 6 selected models. The "Margin" in the feature name indicates that the feature was extracted in the tumor margin. "wavelet.LLH" indicates that the feature calculation was performed on the wavelet-filtered image with a high-pass filter along the cranial-caudal direction and low pass filters along the other two axes, and "glcm" stands for gray level co-occurrence matrix. Kaplan-Meier plots, showing the probability of LF-free survival for high and low risk patients according to the 30 selected RF models are shown in Figure 3. Figures 4 and 5 show the original and wavelet-filtered images for patients at low and high risk according



to Margin\_wavelet.LLH\_glcm\_Correlation. It should be noted that around 66% of the features in the selected models were calculated within the tumor margin. The dominance of tumor margin features is also visible in the final model: Margin\_wavelet.LLH\_glcm\_ClusterProminence (HR: 0.49, CI: 0.32-0.76, p: 0.001), Margin\_wavelet.LLH\_glcm\_Correlation (HR: 0.60, CI: 0.46-0.79, p: 1e-4), wavelet.HLH\_glrIm\_ShortRunHighGrayLevelEmphasis (HR: 0.73, CI: 0.56-0.94, p: 0.01), Margin\_wavelet.HLH\_glcm\_ClusterShade (HR: 0.73, CI: 0.55-0.96, p: 0.02).

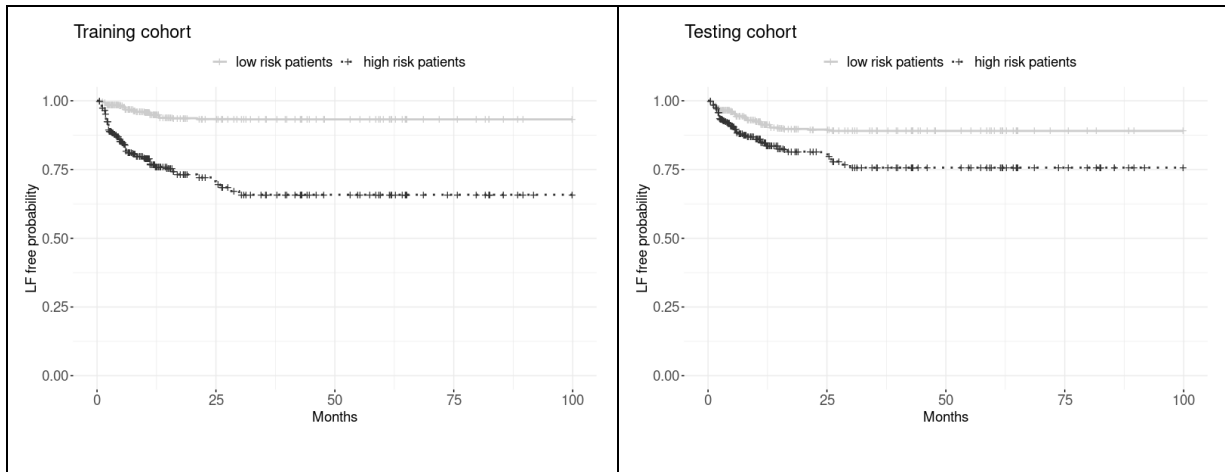


Figure 3: Kaplan-Meier plots for patients at high and low risk of developing local failure (LF) according to the selected radiomic feature models. The figures show the LF-free probabilities for the training (left) and test (right) cohorts over all outer nested cross-validation iterations.

When the features of the clinical, dose and radiomic feature models were fused, no improvement in the performance could be measured. The average c-index of the pipeline was 0.61 +/- 0.12. The prominent features were similar to the ones of the before mentioned models. The 30 selected models contained the features Margin\_wavelet.LLH\_glcm\_Correlation (HR: 0.52 +/- 0.04) 16, gender (HR: 0.41 +/- 0.06) 12 and SysBefore (HR: 0.40 +/- 0.09) 8 times, respectively.

Table 3 - Univariate and multivariate analysis of features (cox-regression). Systemic therapy (variable name: SysBefore) was defined as the application of chemo-, immunotherapy or targeted therapy 14 days before radiotherapy. Abbreviations: CI = 95% confidence interval. \*= Biologically equivalent dose with  $\alpha/\beta$  value of  $\alpha/\beta=10$  Gy)

Variable	Univariate analysis		Multivariate analysis	
	Hazard ratio	p-value	Hazard ratio	p-value
Parallel systemic therapy (SysBefore)	0.37, CI: 0.23-0.58	2e-5	0.49, CI: 0.29-0.82	0.007
Maximum dose*	0.68, CI: 0.52-0.88	0.004	0.84, CI: 0.63-1.13	0.260
Margin_wavelet.LLH_glcm_Correlation	0.55, CI: 0.42-0.70	3e-6	0.64, CI: 0.48-0.85	0.001

Statistical analysis showed that that the gain in performance between dose and radiomics models as well as dose and combined models was significant. The comparison of models with dose and clinical features showed no statistically significant differences. All four model types differed in their performance significantly from a random model with a c-index of 0.5.

An overview of the characteristics of the most relevant clinical, dose and radiomic features, the results of univariate and multivariate Cox regression analyses with SysBefore,  $D_{max}$  and Margin\_wavelet.LLH\_glcm\_Correlation on the entire dataset is shown in Table 3.

#### 4.0 DISCUSSION

The current study provides proof of concept that pre-therapeutic MRI can provide valuable information that may be predictive for treatment outcome in patients with MBM. Our results show that features related to the margin zone of metastases can be associated with treatment outcome and should be implemented in the development of machine learning models for estimating local failure.

Management of MBM requires a multidisciplinary approach to evaluate all available treatment options. Due to the remarkable increase in survival rates since the advent of novel systemic therapy options, controversy is increasing regarding the optimal treatment for MBM (28). In this challenging decision-making process, there is a need for more specific information to predict outcome. To our knowledge, this is the first study to present predictive markers for RT of BM specifically for melanoma in a large, multicenter group of patients. RF analysis could help to

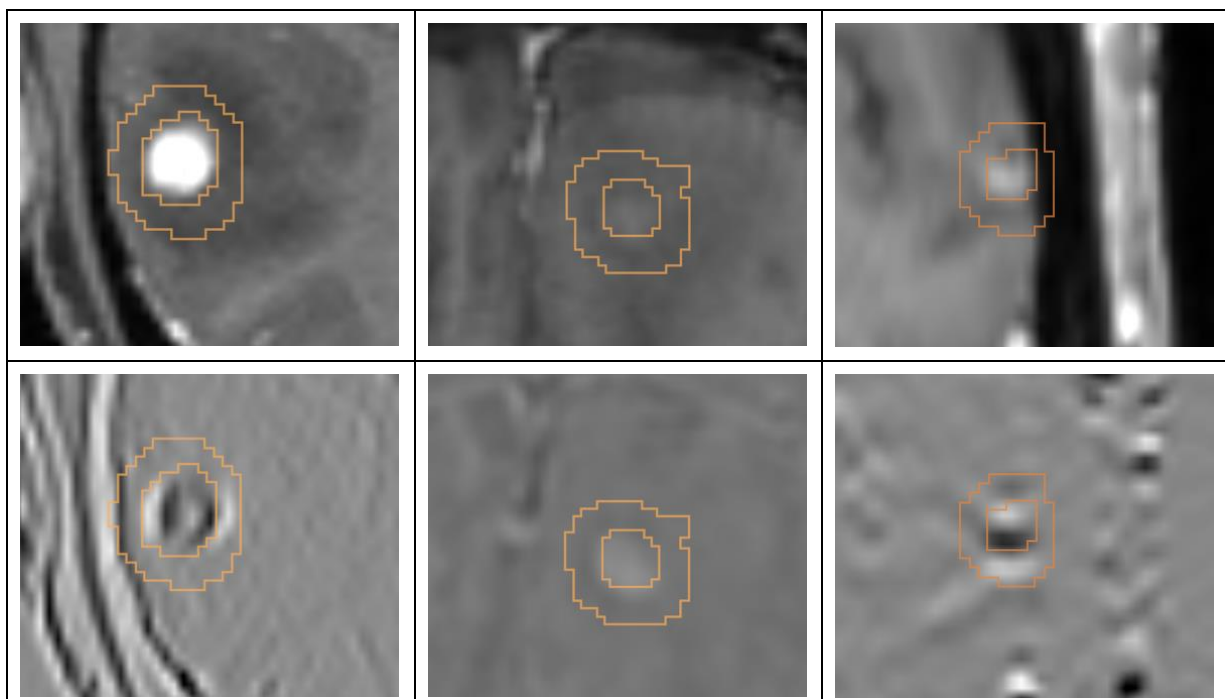


Figure 4: Coronal views of three patients (columns) without local failure at follow-up. The first row shows the original images, the second row shows the wavelet-filtered images with a high-pass along the cranial-caudal axis and low-pass along the other axes. All three patients had a high value for the “Margin\_wavelet.LLH\_glcm\_Correlation”, indicating a low risk of local failure. The contours define the boundary region around the GTV, used to calculate the radiomic feature.

understand the different behavior of metastases by decomposing the underlying tumor lesion characteristics. Margin\_wavelet.LLH\_glcM\_Correlation is the correlation feature of the glcm calculated with the wavelet-filtered MRI and the contour of the tumor margin indicating the linear dependency of gray values. The wavelet filter used a high-pass filter along the cranial-caudal axis and a low-pass filter along the remaining axes, highlighting edges along the high-pass direction. A high correlation can be translated into a high predictability of pixel relationships (29). In the model presented, a high correlation is associated with a lower risk of in-field progression. A reason for a low correlation could be an irregular edge pattern due to vascular or tissue changes. The inclusion of further parameters other than radiomic features could not improve the accuracy of the predictive models in this analysis. This is consistent with the results of Jaberipour et al. who developed a model to predict local failure after radiotherapy in brain metastases with different entities (30).

It is important to note that due to redundancies in the RF set, repeating the analysis with a different cohort could lead to different RF in the models. However, we found a clear trend suggesting that RF extracted from the margin around the tumor contain important information for LF prediction. Around 66% of the features in the selected models for predicting in-field progression were margin features. This suggests that the immediate environment of the metastasis provides information about the probability of recurrence. It is conceivable that features representing contour margin inhomogeneity are associated with more aggressive, infiltrating growth that is not visible on MRI and therefore not covered by the planning target volume. Recent studies have reported peritumoral infiltration in brain metastases at the cellular level histologically using 5-ALA fluorescence (31), which has been shown to have a significant impact on prognosis (32). This infiltration of the brain parenchyma was not associated with

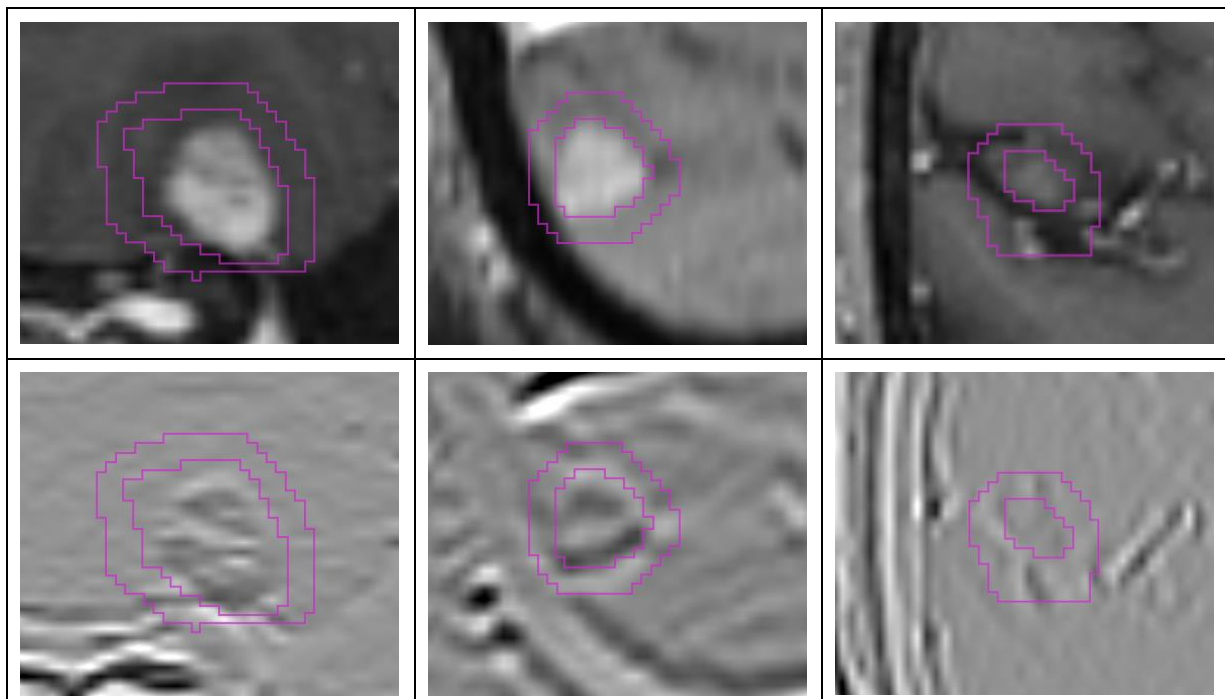


Figure 5: Coronal views of three patients (columns) with local failure after radiotherapy. The first row shows the original images, the second row shows the wavelet-filtered images with a high-pass along the cranial-caudal axis and low pass along the other axes. All three patients had a low value for the feature Margin\_wavelet.LLH\_glcM\_Correlation indicating a high risk of local failure. The contours define the boundary region around the GTV, used to calculate the radiomic feature.

simple MRI parameters such as tumor size, extent of edema, or number of metastases (33). Radiomic analysis has been able to provide information at a cellular and even molecular level (34,35). However, an accurate interpretation of radiomic features remains complicated, and the lack of understanding of different radiomic features is probably the main reason why there are several publications presenting robust radiomics, but none regarding their clinical implementation. Histopathological studies could investigate a possible correlation between radiomic features and infiltration on a cellular level.

We identified RF associated with outcome despite using imaging data from different institutions and imaging devices. The lack of standardized MRI acquisition parameters reflects a real-world problem. Our model was trained and validated on routinely acquired 3D-Gd<sup>T1w</sup>-MRI and does not require a standardized acquisition protocol with multiple sequences. This facilitates the review and implementation process into clinical routine for other institutions. This is highly relevant as there is a need for multicenter, collaborative studies. Nevertheless, analysis of additional sequences may reveal further imaging markers and standardized protocols may be helpful in developing more accurate models.

A potential limitation of this study is the nested cross-validation method. It allows for model selection and performance estimation on independent test-sets and is more robust than simple cross-validation or single train and test-sets, which can be found frequently in literature (34,36). Nevertheless, the sensitivity of the pipeline to dataset shifts cannot be measured as in an evaluation with independent datasets (27). On the other hand, we aimed for vendor- and center-independent radiomic features, which could only be achieved with a heterogeneous reference dataset. For these reasons and the relatively small size of the single datasets, we did not use the external datasets as independent test sets. Larger multicentric data sets are needed in further research to ensure generalizability.

In conclusion, the analysis of radiomic features on pretherapeutic MRI can provide critical, additional information to predict local failure after radiotherapy of MBM. The most prominent features in the model-building pipeline were related to the direct margin around the metastases, which is likely to provide information on the probability of recurrence. This may help to *a priori* identify metastases with a higher risk of local failure. The applicability to brain metastases of other entities needs to be tested in further analyses. In the future, these findings could contribute to more individualized radiotherapy, e.g. larger margins, combination therapies or dose-escalation in high-risk-lesions.

## References

1. Davies MA, Liu P, McIntyre S, Kim KB, Papadopoulos N, Hwu WJ, u. a. Prognostic factors for survival in melanoma patients with brain metastases. *Cancer*. 15. April 2011;117(8):1687–96.
2. Fife KM, Colman MH, Stevens GN, Firth IC, Moon D, Shannon KF, u. a. Determinants of Outcome in Melanoma Patients With Cerebral Metastases. *JCO*. 1. April 2004;22(7):1293–300.
3. Schadendorf D, van Akkooi ACJ, Berking C, Griewank KG, Gutzmer R, Hauschild A, u. a. Melanoma. *The Lancet*. September 2018;392(10151):971–84.
4. Neal MT, Chan MD, Lucas JT, Loganathan A, Dillingham C, Pan E, u. a. Predictors of Survival, Neurologic Death, Local Failure, and Distant Failure After Gamma Knife Radiosurgery for Melanoma Brain Metastases. *World Neurosurgery*. Dezember 2014;82(6):1250–5.
5. Reese RA, Lamba N, Catalano PJ, Cagney DN, Wen PY, Aizer AA. Incidence and Predictors of Neurologic Death in Patients with Brain Metastases. *World Neurosurgery*. 1. Juni 2022;162:e401–15.
6. Eigentler TK, Figl A, Krex D, Mohr P, Mauch C, Rass K, u. a. Number of metastases, serum lactate dehydrogenase level, and type of treatment are prognostic factors in patients with brain metastases of malignant melanoma. *Cancer*. 15. April 2011;117(8):1697–703.
7. Raizer JJ, Hwu WJ, Panageas KS, Wilton A, Baldwin DE, Bailey E, u. a. Brain and leptomeningeal metastases from cutaneous melanoma: Survival outcomes based on clinical features. *Neuro-Oncology*. 1. April 2008;10(2):199–207.
8. Hasegawa T, Kondziolka D, Flickinger JC, Germanwala A, Lunsford LD. Brain Metastases Treated with Radiosurgery Alone: An Alternative to Whole Brain Radiotherapy? *Neurosurgery*. Juni 2003;52(6):1318–26.
9. Ghia AJ, Tward JD, Anker CJ, Boucher KM, Jensen RL, Shrieve DC. Radiosurgery for melanoma brain metastases: the impact of hemorrhage on local control. *J Radiosurg SBRT*. 2014;3(1):43–50.
10. Ramakrishna N, Margolin KA. Multidisciplinary Approach to Brain Metastasis from Melanoma; Local Therapies for Central Nervous System Metastases. *American Society of Clinical Oncology Educational Book*. Mai 2013;(33):399–403.
11. Yamamoto M, Higuchi Y, Sato Y, Aiyama H, Kasuya H, Barford BE. Stereotactic Radiosurgery for Patients with 10 or More Brain Metastases. *Prog Neurol Surg*. 2019;34:110–24.
12. Gondi V, Pugh SL, Tome WA, Caine C, Corn B, Kanner A, u. a. Preservation of Memory With Conformal Avoidance of the Hippocampal Neural Stem-Cell Compartment During Whole-Brain Radiotherapy for Brain Metastases (RTOG 0933): A Phase II Multi-Institutional Trial. *JCO*. 1. Dezember 2014;32(34):3810–6.
13. Sperduto PW, Jiang W, Brown PD, Braunstein S, Sneed P, Wattson DA, u. a. Estimating Survival in Melanoma Patients With Brain Metastases: An Update of the Graded Prognostic Assessment for Melanoma Using Molecular Markers (Melanoma-molGPA). *International Journal of Radiation Oncology\*Biophysics*. November 2017;99(4):812–6.
14. Bian SX, Routman D, Liu J, Yang D, Groshen S, Zada G, u. a. Prognostic factors for melanoma brain metastases treated with stereotactic radiosurgery. *JNS*. Dezember 2016;125(Supplement\_1):31–9.
15. Stera S, Balampas P, Blanck O, Wolff R, Wurster S, Baumann R, u. a. Stereotactic radiosurgery combined with immune checkpoint inhibitors or kinase inhibitors for patients

- with multiple brain metastases of malignant melanoma. *Melanoma Research*. April 2019;29(2):187–95.
16. Rizzo S, Botta F, Raimondi S, Origi D, Fanciullo C, Morganti AG, u. a. Radiomics: the facts and the challenges of image analysis. *Eur Radiol Exp*. Dezember 2018;2(1):36.
  17. Bhatia A, Birger M, Veeraraghavan H, Um H, Tixier F, McKenney AS, u. a. MRI radiomic features are associated with survival in melanoma brain metastases treated with immune checkpoint inhibitors. *Neuro-Oncology*. 17. Dezember 2019;21(12):1578–86.
  18. Lin NU, Lee EQ, Aoyama H, Barani IJ, Barboriak DP, Baumert BG, u. a. Response assessment criteria for brain metastases: proposal from the RANO group. *Lancet Oncol*. Juni 2015;16(6):e270-278.
  19. Cox DR. Regression models and life-tables. *Journal of the Royal Statistical Society: Series B (Methodological)*. 1972;34(2):187–202.
  20. Grosu AL, Frings L, Bentsalo I, Oehlke O, Brenner F, Bilger A, u. a. Whole-brain irradiation with hippocampal sparing and dose escalation on metastases: neurocognitive testing and biological imaging (HIPPORAD) – a phase II prospective randomized multicenter trial (NOA-14, ARO 2015–3, DKTK-ROG). *BMC Cancer*. Dezember 2020;20(1):532.
  21. Carré A, Klausner G, Edjlali M, Lerousseau M, Briend-Diop J, Sun R, u. a. Standardization of brain MR images across machines and protocols: bridging the gap for MRI-based radiomics. *Sci Rep*. 23. Juli 2020;10(1):12340.
  22. Avants B, Tustison NJ, Song G. Advanced Normalization Tools: V1.0. *The Insight Journal* [Internet]. 29. Juli 2009 [zitiert 17. März 2023]; Verfügbar unter: <https://www.insight-journal.org/browse/publication/681>
  23. Smith SM. Fast robust automated brain extraction. *Hum Brain Mapp*. November 2002;17(3):143–55.
  24. Isensee F, Jaeger PF, Kohl SAA, Petersen J, Maier-Hein KH. nnU-Net: a self-configuring method for deep learning-based biomedical image segmentation. *Nat Methods*. Februar 2021;18(2):203–11.
  25. Karami E, Soliman H, Ruschin M, Sahgal A, Myrehaug S, Tseng CL, u. a. Quantitative MRI Biomarkers of Stereotactic Radiotherapy Outcome in Brain Metastasis. *Sci Rep*. 27. Dezember 2019;9(1):19830.
  26. van Griethuysen JJM, Fedorov A, Parmar C, Hosny A, Aucoin N, Narayan V, u. a. Computational Radiomics System to Decode the Radiographic Phenotype. *Cancer Research*. 1. November 2017;77(21):e104–7.
  27. Bradshaw TJ, Huemann Z, Hu J, Rahmim A. A Guide to Cross-Validation for Artificial Intelligence in Medical Imaging. *Radiology: Artificial Intelligence*. Juli 2023;5(4):e220232.
  28. Kruser TJ, Gondi V, Sperduto PW, Brown PD, Mehta MP. Omitting radiosurgery in melanoma brain metastases: a drastic and dangerous de-escalation. *The Lancet Oncology*. August 2018;19(8):e366.
  29. Mryka Hall-Beyer. GLCM Texture: A Tutorial v. 3.0 March 2017. 2017 [zitiert 14. Februar 2023]; Verfügbar unter: <http://rgdoi.net/10.13140/RG.2.2.12424.21767>
  30. Jaberipour M, Soliman H, Sahgal A, Sadeghi-Naini A. A priori prediction of local failure in brain metastasis after hypo-fractionated stereotactic radiotherapy using quantitative MRI and machine learning. *Sci Rep*. 3. November 2021;11:21620.
  31. Schatlo B, Stockhammer F, Barrantes-Freer A, Bleckmann A, Siam L, Pukrop T, u. a. 5-Aminolevulinic Acid Fluorescence Indicates Perilesional Brain Infiltration in Brain Metastases. *World Neurosurgery*: X. Januar 2020;5:100069.
  32. Siam L, Bleckmann A, Chaung HN, Mohr A, Klemm F, Barrantes-Freer A, u. a. The metastatic infiltration at the metastasis/brain parenchyma-interface is very heterogeneous

and has a significant impact on survival in a prospective study. *Oncotarget*. 6. Oktober 2015;6(30):29254–67.

33. Fiss I, Hussein A, Barrantes-Freer A, Sperling S, Hernandez-Duran S, Wolfert C, u. a. Cerebral metastases: do size, peritumoral edema, or multiplicity predict infiltration into brain parenchyma? *Acta Neurochir*. Mai 2019;161(5):1037–45.

34. Shofty B, Artzi M, Shtrozberg S, Fanizzi C, DiMeco F, Haim O, u. a. Virtual biopsy using MRI radiomics for prediction of BRAF status in melanoma brain metastasis. *Sci Rep*. 20. April 2020;10(1):6623.

35. Su CQ, Chen XT, Duan SF, Zhang JX, You YP, Lu SS, u. a. A radiomics-based model to differentiate glioblastoma from solitary brain metastases. *Clinical Radiology*. August 2021;76(8):629.e11-629.e18.

36. Mouraviev A, Detsky J, Sahgal A, Ruschin M, Lee YK, Karam I, u. a. Use of radiomics for the prediction of local control of brain metastases after stereotactic radiosurgery. *Neuro-Oncology*. 2020;22(6):797–805.

## Supplementary material I

### MRI acquisition specifications for 3D-GdT1w-MRI

Manufacturer and System		Field strength	Voxel size [mm]	Image matrix	TR [ms]	TE [ms]	FA [°]	Slice thickness [mm]
SIEMENS	Avanto	1.5	0.5	512x512	2050	3.02	15	1
SIEMENS	Avanto_fit	1.5	0.49	512x512	1930	4.83	15	1
SIEMENS	Espreo	1.5	0.5	512x512	1900	2.56	15	1
SIEMENS	MAGNETOM vida	3	0.9	256x256	2300	3.55	8	1
SIEMENS	Prisma	3	1	256x256	2300	2.26	12	1
SIEMENS	Symphony	1.5	0.5	512x512	1890	4.38	12	1
SIEMENS	Symphony	1.5	0.5	512x512	1799	3.93	15	1
SIEMENS	TrioTrim	3	0.5	512x512	2200	2.15	12	1
SIEMENS	TrioTrim	3	0.5	512x512	1390	2.15	15	1
Philips	Achieva	1.5	0.8	512x512	25	1.9	30	1.5
Philips	Achieva dStream	3	0.68	251x251	700	30	80	1
Philips	Ingenia	3	0.71	252x252	9	3.99	8	1

## Supplementary material II

A prerequisite for a robust radiomics model is, that the RFs are not affected by inter-observer variability of the contours. However, since only one expert contour per lesion was available, three additional artificial contour datasets to simulate additional observers were created. One artificial contour datasets was created by facilitating the nnUnet trained on 57 MR images and corresponding expert contours the Center I. The network was tested on 20 other patients with a total of 58 lesions. The network detected 52 lesions which corresponds to a sensitivity of 90 %. A comparison of the detected lesions with the expert contours yielded a median Sørensen-Dice coefficient of 0.82. The other two artificial contour datasets were made by applying either a morphological erosion, morphological dilation or identity function to each of the expert contours. Which of these three function was used for a certain contour was random.

## Supplementary material III

RF were calculated using Pyradiomics v3.0.1 with a fixed bin count of 32 for the original and the wavelet filtered images. For the remaining parameters the default values were used to calculate features of the following feature classes: shape, firstorder, glcm (grey-level co-occurrence matrix), glrlm (grey-level run-length matrix), glszm (grey-level size zone matrix), glldm (grey-level dependence matrix).

To reduce the risk of overfitting the number of features was reduced by the following steps:

1. Contour dependency: Only features with similar distributions (see statistical details) for all four contour sets were retained.
2. Univariate analysis: First, all features that did not meet the assumptions of the Cox Proportional Hazards Model (CPHM) or had zero variance were eliminated. Second, a univariate CPHM was trained for each feature on the training set. Features that did not have a model coefficient significantly different from zero were excluded.
3. Feature clustering: A hierarchical tree with 1-Spearman correlation coefficient as distance and complete linkage was constructed and cut at a height of 0.2. From each cluster, the RF with the lowest p-value according to the univariate CPHM from step 2 was retained.